Article

Not peer-reviewed version

An Acid Responsive Fluorescent Molecule for Erasable Anti-Counterfeiting

Jiabao Liu , Xiangyu Gao , Qingyu Niu , Mingyuan Jin , Yijin Wang , Thamraa Alshahrani , He-Lue Sun , Banglin Chen , Zhiqiang Li * , Peng Li *

Posted Date: 2 August 2024

doi: 10.20944/preprints202408.0049.v1

Keywords: aggregation-induced emission; stimuli-responsive luminescence; diaminotriazine; anti-counterfeiting

Article

An Acid Responsive Fluorescent Molecule for Erasable Anti-Counterfeiting

Jiabao Liu, [1] Xiangyu Gao, [2] Qingyu Niu, [1] Mingyuan Jin, [3] Yijin Wang, [2] Thamraa Alshahrani, [4] He-Lue Sun, [3] Banglin Chen, [5] Zhiqiang Li [1,*] and Peng Li [2,*]

[1] School of Chemical Engineering and Technology, Hebei University of Technology, Tianjin 300130, China
[2] Shanghai Key Laboratory of Molecular Catalysis and Innovative Materials, Fudan University, Shanghai 200438, China
[3] College of Chemistry and Materials Science, Hebei Normal University, Shijiazhuang, 050024, China
[4] Department of Physics, College of Science, Princess Nourah bint Abdulrahman University, Riyadh, 11671, Saudi Arabia
[5] Fujian Provincial Key Laboratory of Polymer Materials, College of Chemistry & Materials Science, Fujian Normal University, Fuzhou, Fujian, 350000, China
* Correspondence: zhiqiangli@hebut.edu.cn (Z.L.); penglichem@fudan.edu.cn (P.L.)

Abstract: A tetraphenylethylene-derived compound, **TPEPhDAT**, has been prepared by successive Suzuki-Miyaura coupling and ring-closing reactions. This compound exhibits aggregation-induced emission (AIE) properties in the DMSO/MeOH system, with a fluorescence emission intensity in the aggregated state that is 5-fold higher than that of its counterpart in a dilute solution. Moreover, the diaminotriazine structure of the molecule is a good acceptor of protons, and thus the **TPEPhDAT** molecule exhibits acid-responsive fluorescence. **TPEPhDAT** was protonated by trifluoroacetic acid (TFA), leading to a fluorescence quenching, which was reversibly restored by treatment with ammonia (On-Off switch). Time-dependent density functional theory (TDDFT) computational studies have shown that protonation enhances the electron-withdrawing capacity of the triazine nucleus and reduces the bandgap, producing a more intense intramolecular charge transfer (ICT), thus leading to fluorescence quenching. MeOH can easily remove the protonated **TPEPhDAT**, and this acid-induced discolouration and erasable property can be applied in anti-counterfeiting.

Keywords: aggregation-induced emission; stimuli-responsive luminescence; diaminotriazine; anti-counterfeiting

1. Introduction

Stimuli-responsive luminescent materials are materials with intelligent response characteristics that can change their fluorescent colour by external stimuli such as force[1,2], temperature[3-5], pH[6,7], light[8-11], magnetic field[12], etc[13-15]. Among them acid stimulus-responsive fluorescent materials play a crucial role in anti-counterfeiting and security. Adding acid-stimuli-responsive fluorescent materials to a label changes the colour or pattern of the label when exposed to acid. This can be used to protect products from counterfeiting and tampering[16,17]. Developing acid-stimulation responsive materials that reveal hidden information when exposed to acidic environments[18,19]. This can be used to create anti-counterfeiting documents and security markings.

The controlled erasure of fluorescent molecules is crucial for securely transmitting encrypted information. However, most current research on erasable materials still relies on the attenuation of fluorescent signals. The development of molecular materials that can be removed with common solvents presents a more convenient method for tamper-resistant removal. Nevertheless, this method of conveniently erasing information still requires further improvement[20-23].

Most systems discussed so far suffer from the aggregation-caused quenching (ACQ) effect, which is very limited in practical applications involving solid substrates. On the other hand, aggregation-induced emission (AIE) molecules, which Tang and coworkers pioneered[24,25], emit

 doi:10.20944/preprints202408.0049.v1

bright fluorescence in the solid or aggregated state but usually show weak or even no fluorescence in solution, which endows solid materials with fascinating fluorescent properties. Therefore, introducing AIE properties into smart response anti-counterfeiting materials is an ideal strategy to solve the limitations of ACQ.

Therefore, we have designed a tetraphenylethylene (TPE)-based molecule decorated with diaminotriazine (DAT) groups, which shows strong AIE properties and can hardly dissolve in any common solvent. However, the molecule can easily react with various organic and inorganic acids by protonating the N atoms in the triazine rings. Over 90% or more fluorescence diminution occurs upon reaction, while **TPEPhDAT**, after protonation, can be quickly removed with common MeOH solvents. We demonstrate that this material can be processed into paper with encrypted information for anti-counterfeiting applications by solution methods.

2. Results and Discussion

*2.1. Synthesis and Structural Elucidation of **TPEPhDAT***

TPEPhDAT was synthesized according to a previous report and was obtained by a two-step reaction[26,27], the synthetic route of which is shown in Scheme 1. 1,1,2,2-tetrakis(4-bromophenyl)ethene and 4-cyanophenylboronic acid underwent Suzuki-Miyaura coupling to obtain extended **TPEPhCN**. The yellowish **TPEPhDAT** could be easily obtained in 80% yield by reacting the corresponding nitrile with dicyandiamide. The structure of **TPEPhDAT** was characterized and confirmed by ^{1}H NMR and ^{13}C NMR (Figures S1–S4).

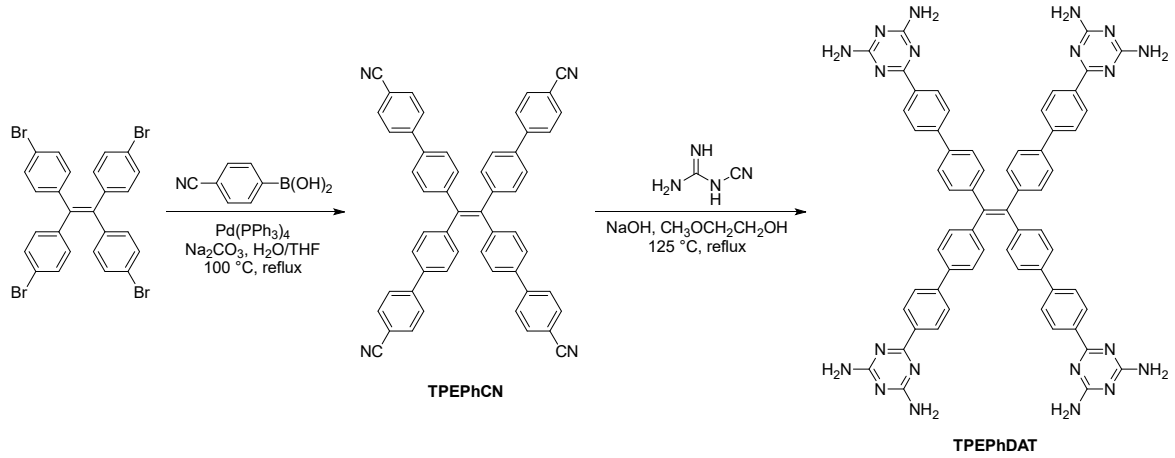

Scheme 1. Synthesis and characterization of **TPEPhDAT**.

*2.2. AIE Characteristic of **TPEPhDAT***

The AIE properties of **TPEPhDAT** were explored in the DMSO/MeOH system (Figure 1a). In this system, DMSO is a good solvent, and MeOH is a poor solvent. The luminescence of **TPEPhDAT** is extremely weak in pure DMSO, when the volume fraction of MeOH (f_{MeOH}) was increased from 0 vol% to 30 vol%, the fluorescence emission spectra were continuously blue-shifted and the intensity of the emission peaks decreased slightly. This particular fluorescence change has been identified in existing reports[28-30], and this phenomenon can be attributed to suppression of proximity effect (SOPE)[31,32]. When f_{MeOH} was greater than 30 vol%, the intensity of the emission peaks was gradually enhanced, reaching a maximum at f_{MeOH} of 95 vol% (Figure 1b). Compared with the pure DMSO system, the fluorescence intensity increased about 5-fold (Figure 1c). Besides, the fluorescence spectra of the aggregates were blue-shifted compared with that of the solution (Figure 1b). The above phenomenon results from the joint action of the solvation effect and AIE effect[33-35].

 doi:10.20944/preprints202408.0049.v1

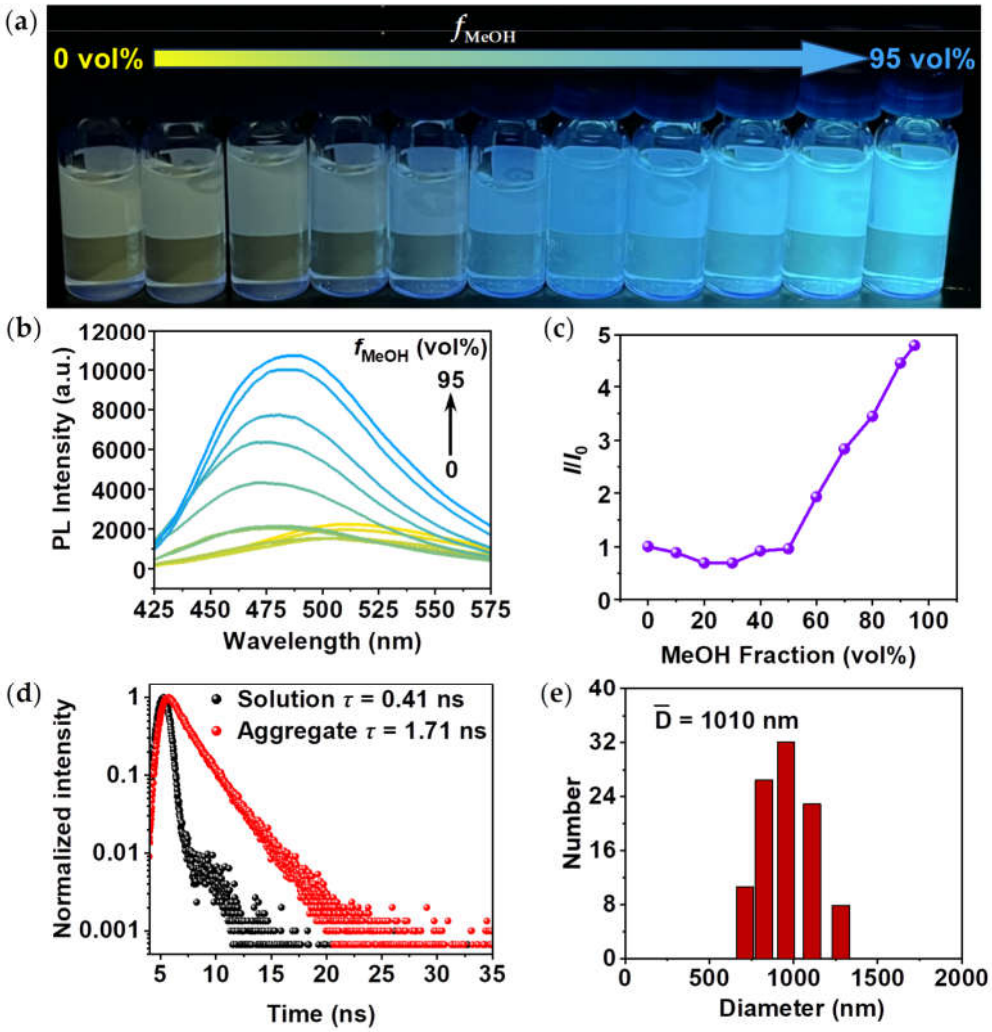

Figure 1. (**a**) Photograph of the volume fraction of MeOH (f_{MeOH}) increasing from 0 vol% to 95 vol% (under UV light); (**b**) Fluorescence spectra of **TPEPhDAT** in DMSO/MeOH mixtures with different f_{MeOH} (concentration: 10 μM; excitation wavelength: 380 nm); (**c**) Plot of relative PL intensity (I/I_0) *vs* f_{MeOH}; (**d**) Time-resolved decay curves of solution (f_{MeOH} = 0 vol%) and aggregate (f_{MeOH} = 95 vol%) at λ_{ex} = 350 nm, these curves were fitted according to a double exponential function ($I = I_0 + A_1\exp(-t/\tau_1) + A_2\exp(-t/\tau_2)$, black: $I = 2.03\times10^{-4} + 279730\exp(-t/0.41) + 365767\exp(-t/0.41)$; red: $I = 1.18\times10^{-4} + 31.25\exp(-t/1.59) + 1.55\exp(-t/3.22)$); (**e**) Hydrodynamic radius distribution of **TPEPhDAT** in DMSO/MeOH mixtures.

In dilute DMSO solution, the benzene ring rotor of TPE undergoes dynamic intramolecular rotation, and the excited state energy is dissipated in the form of non-radiative leaps, resulting in weak luminescence. As the f_{MeOH} increases, the molecule appears aggregated, and the rotation of the benzene ring rotor is spatially limited. The restricted intramolecular rotation (RIR) suppresses the abovementioned non-radiative decay[24,36], and the excited state molecules can only return to the ground state by radiative decay, significantly enhancing the fluorescence. When f_{MeOH} = 95 vol%, the absorption intensity of the ultraviolet-visible (UV-vis) spectra underwent a significant decrease, and at the same time, the tail elevation phenomenon appeared at the long wavelength band of the absorption spectrum (Figure S5), indicating that the addition of MeOH caused the aggregation of **TPEPhDAT** in the system[37,38]. Figure 1d shows the fluorescence lifetime decay curves of **TPEPhDAT** in DMSO solution and DMSO/MeOH mixture (f_{MeOH} = 95 vol%). The τ value of **TPEPhDAT** increases from 0.41 ns to 1.71 ns as the MeOH fraction in the mix is increased from 0 vol% to 95 vol%. The longer fluorescence lifetime reflects that **TPEPhDAT** is more immobilized and aggregated[39,40]. In the meantime, when f_{MeOH} = 95 vol%, aggregates with a hydrodynamic diameter

 doi:10.20944/preprints202408.0049.v1

of about 1 μm appeared, as confirmed by dynamic light scattering (DLS, Figure 1e) and scanning electron microscopy (SEM, Figure S6).

2.3. Acidochromism

The nitrogen atoms in the DAT moiety are considered effective proton acceptors[7,41,42]. Given this, we investigated the possible acid-induced fluorescence discolouration properties of **TPEPhDAT**. In an aqueous dispersion of **TPEPhDAT**, an excess of HNO_3 was added dropwise, and an immediate change in fluorescence was observed (Figure 2a). As shown in Figure 2b, the aqueous dispersion of **TPEPhDAT** showed bright yellow fluorescence with the maximum emission peak at 522 nm (λ_{ex} = 350 nm). In contrast, the dropwise addition of HNO_3 completely disappeared the initial emission band at 522 nm, and a new peak at 549 nm corresponded to the orange emission. The fluorescence of **TPEPhDAT+HNO$_3$** was extremely weak, and the quenching rate reached 95%. In addition, we also discussed the acid-induced fluorescence discolouration properties of four acids, including HCl, trifluoroacetic acid (TFA), H_2SO_4, and formic acid (FA), in addition to HNO_3 (Figure S7). The results showed that similar results were presented with HNO_3, and the quenching efficiency of HCl, H_2SO_4, and TFA could reach more than 85%, while FA was less acidic, and the quenching efficiency could only reach 61% (Figure 2c). The results of the absolute quantum yield (Φ) tests are in close agreement with those of the fluorescence quenching (Figure S8). In an aqueous solution, the Φ of **TPEPhDAT** can reach 57.36%, which decreases to different degrees after adding different acids, especially after adding HNO_3. The Φ can be reduced to 6.85%. It is proved that the fluorescence change of **TPEPhDAT** is caused by hydrogen ions (H^+) but not by anions (NO_3^-), and the stronger the acidity, the more pronounced the effect of acid discolouration.

We attempted to treat acidified **TPEPhDAT** with ammonia. We found that the addition of excess ammonia fully restored the fluorescence, which was still fully restored after four cycles of repeated treatment with TFA and ammonia (Figure 2d). When the solution was treated with TFA and ammonia alternately, the fluorescence emission could be switched several times between "off and on" states. This implies that the reaction is entirely reversible.

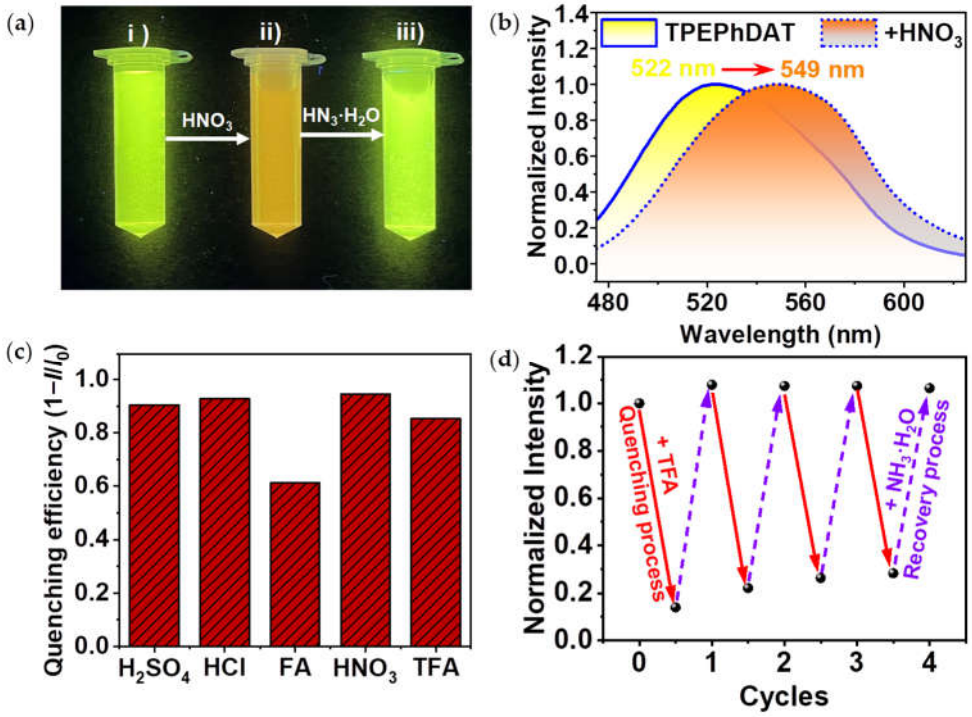

Figure 2. (**a**) Pictures of acid-responsive fluorescence color changes (under UV light) of **TPEPhDAT** i) in its original state, ii) after dropwise addition of 0.5 M HNO_3, and iii) after dropwise addition of ammonium hydroxide; (**b**) Fluorescence spectra of **TPEPhDAT** under 350 nm excitation before and after dropwise addition of 0.5 M HNO_3; (**c**) Fluorescence quenching efficiency of **TPEPhDAT** with the

 doi:10.20944/preprints202408.0049.v1

addition of different acids; (**d**) Fluorescence recovery cycle of **TPEPhDAT** to TFA: the red solid line indicates the quenching process and the purple dashed line indicates the recovery process.

*2.4. Mechanism of **TPEPhDAT** Binding to Acid*

To further understand the binding behaviour at the molecular level, we performed ^{1}H NMR measurements using TFA as an example. The two protons of −NH_2 in **TPEPhDAT** show a single broad peak. In contrast, after being protonated, these two protons show two separate single peaks that shifted to a lower field than before protonation (Figure 3a). The non-equivalence of the two amino protons is because the bond between C-4 and −NH_2 has a partially double-bonded nature after being protonated, resulting in a blockage of its rotation (Figure S9)[43,44].

This suggests that the protonation of **TPEPhDAT** occurs on the triazine ring and not on −NH_2. Fourier transform infrared (FT-IR) spectroscopy further confirms this. As shown in Figure 3b, the peaks at 1582 and 814 cm^{-1} significantly shift to 1560 and 797 cm^{-1} upon the addition of TFA. These changes are attributed to the deformation of the triazine ring from an ideal hexagonal shape upon protonation[45-47]. The peaks of deprotonated −COOH were also observed (1676 and 1385 cm^{-1})[48]. This indicates that upon the reaction of TFA with **TPEPhDAT**, the −COOH of TFA loses its proton and forms $-COO^-$. The changes in FT-IR spectra provided evidence for the protonation of the triazine ring. In aqueous solutions, triazine cyclonitrogen is generally more alkaline than nitrogen in −NH_2[49-52], because its lone pair electrons do not participate in conjugation and are more vulnerable to proton attack. In addition, the strong electron absorption of the triazine ring causes the electronegativity of amino nitrogen to easily transfer to the triazine ring (Figure S10)[53], preventing amino nitrogen from binding with protons.

Given this, we prepared co-crystals of **TPEPhDAT** with TFA by solvothermal methods (Figure S11). As can be seen from the crystal structure (Figure 3c; Figure S12, Table S1), the protonation of **TPEPhDAT** occurs on the triazine ring rather than on −NH_2. This crystal structure provides a possible site for the binding of **TPEPhDAT** to acids.

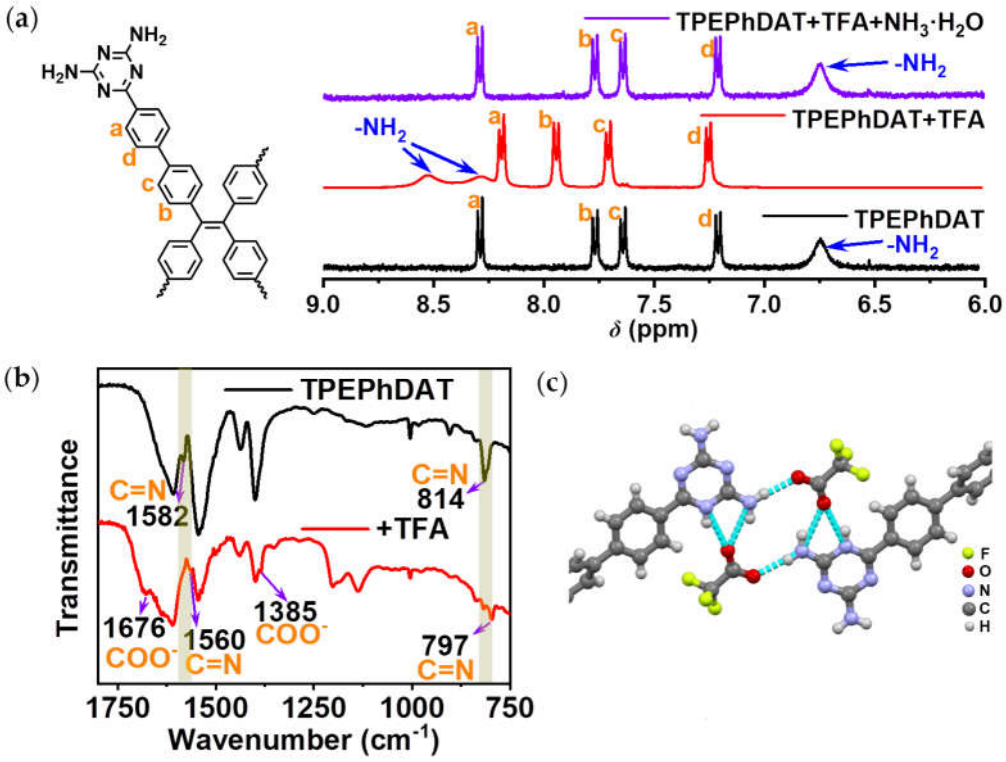

Figure 3. (**a**) Partial ^{1}H NMR spectra of **TPEPhDAT** in DMSO-d_6 after adding TFA and NH_3·H_2O; (**b**) FT-IR spectra of **TPEPhDAT** before and after protonation; (**c**) DAT moiety interacts with the TFA portion.

 doi:10.20944/preprints202408.0049.v1

*2.5. Possible Mechanism of Acid-induced Fluorescence Quenching in **TPEPhDAT***

As can be seen in Figure 4a, the **TPEPhDAT** molecule has weak intramolecular charge transfer (ICT) properties. When **TPEPhDAT** reacts with TFA, the triazine ring exhibits a strong nucleophilic ability and can effectively attack the −COOH of TFA to generate the corresponding salt. Upon completion of protonation, the ICT effect of **TPEPhDAT** was enhanced, achieving a significant change in fluorescence from the initial yellow to orange[54,55]. Therefore, simple deprotonation methods can help restore the probe's fluorescence properties. For example, **TPEPhDAT** can be simply deprotonated by adding ammonia, thus restoring the initial properties of the fluorescent probe.

To elucidate the chemical sensing system's quenching mechanism, time-resolved fluorescence spectroscopy was utilized to investigate the quenching dynamics (Figure 4b). The results revealed that the fluorescence lifetimes of **TPEPhDAT** were 2.29 ns and 0.62 ns before and after adding 0.25 M H_2SO_4, respectively, indicating a dynamic quenching process[56]. Furthermore, simple deprotonation treatment can restore the fluorescence of **TPEPhDAT**; for instance, dropping ammonia can restore the fluorescence lifetime to its initial state (2.10 ns).

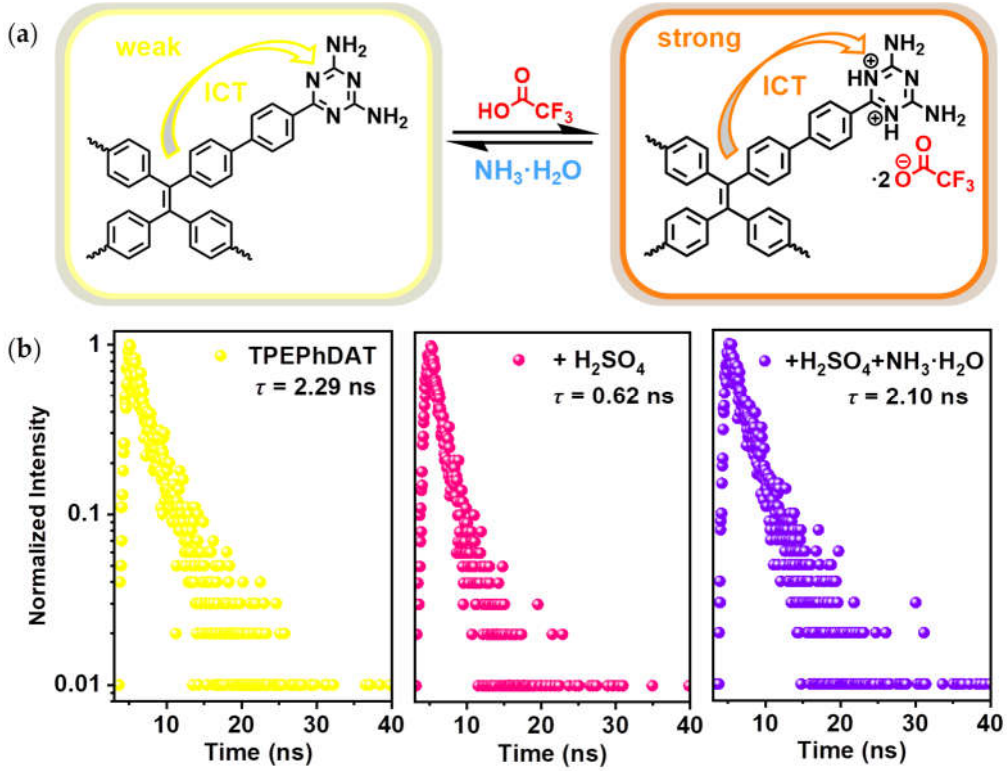

Figure 4. (**a**) Supposed sensing mechanism of **TPEPhDAT** to TFA; (**b**) Time-resolved decay curves of **TPEPhDAT** after successive treatment by TFA and ammonia at λ_{ex} = 350 nm, these curves were fitted according to a triple exponential function ($I = I_0 + A_1\exp(-t/\tau_1) + A_2\exp(-t/\tau_2) + A_3\exp(-t/\tau_3)$, yellow: I = 1.96×10^{-4} + 3.32exp(−t/1.61) + 7.10exp(−t/1.61) 1.51exp(−t/4.13); magenta: I = 2.42×10^{-4} + 1.82exp(−t/3.94) + 6.99exp(−t/1.39) + 8.82exp(−t/1.39); purple: I = 1.87×10^{-4} + 1877exp(−t/0.59) + 0.68exp(−t/3.68) + 15.09exp(−t/1.56).

In addition, we have investigated the mechanism by which TFA quenches the fluorescence of **TPEPhDAT** by time-dependent density functional theory (TDDFT) calculations. As shown in Figure 5, on the natural transition orbitals (NTOs) of the bare **TPEPhDAT** probe, most of the "hole" of **TPEPhDAT** is localized on the TPE units of the backbone. At the same time, the "particle" of **TPEPhDAT** is distributed throughout the molecular backbone. This result fits well with the weak ICT state of the $S_0 \rightarrow S_1$ transition in the **TPEPhDAT** molecule. After protonation, it can be seen that the "hole" is mainly located on the TPE unit, which is similar to the **TPEPhDAT** probe before protonation. In contrast, in the $S_0 \rightarrow S_1$ transition, the "particle" is mainly located on the triazine ring

 doi:10.20944/preprints202408.0049.v1

unit of the backbone. As a result, a large orbital separation between the hole and the particle is observed, and the oscillator strength (*f*) correspondingly decreases from 0.8926 for the bare **TPEPhDAT** probe to 0.3359 for the protonated **TPEPhDAT** probe. The molecular energy is also reduced simultaneously after protonation (Figure S13). These results indicate that the protonated **TPEPhDAT** probe has stronger ICT properties[17,57]. This shows that the theoretical calculations agree with the sensing mechanism."

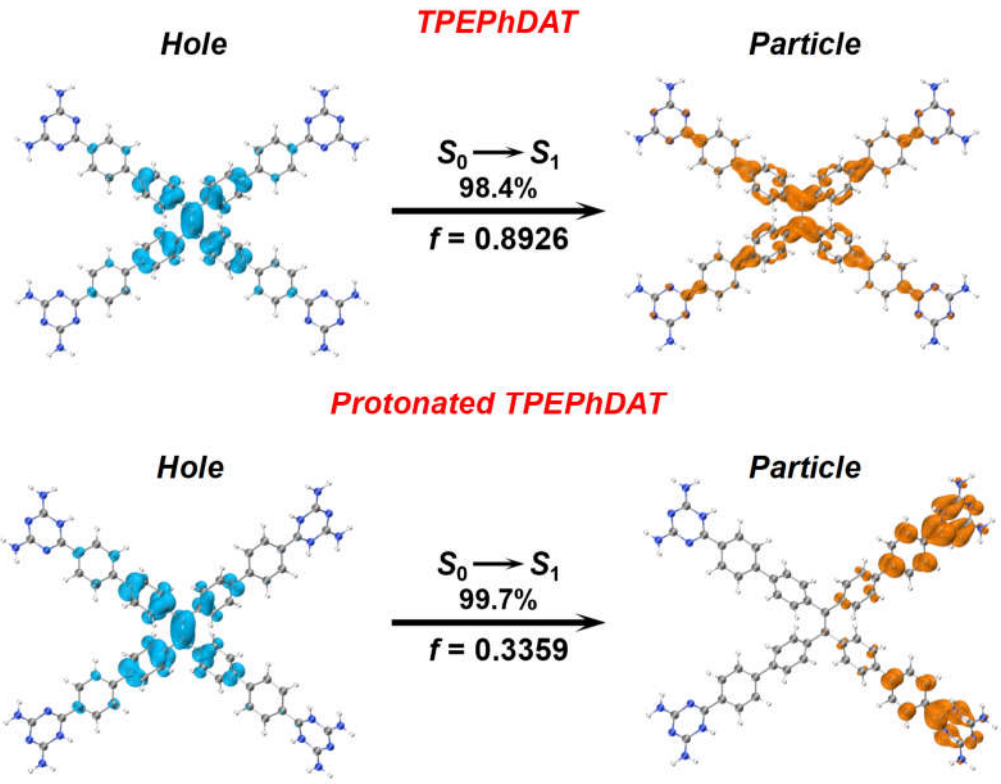

Figure 5. TDDFT calculations and $S_0 \rightarrow S_1$ NTO calculations for **TPEPhDAT**. Protonation is adopted to simulate TFA stimulation, as previously reported.

Generally, the fluorescence lifetime of the molecule increases with the enhancement of ICT[58]. However, the fluorescence lifetime decreases after protonation, and ICT enhancement increases the molecule's dipole moment, which leads to a decrease in the energy difference between the excited and ground states. As a result, excited state electrons are more likely to return to the ground state via nonradiative pathways, thereby shortening the fluorescence lifetime. As shown in Figure S14, after the **TPEPhDAT** proton, the dihedral angle between the DAT group and the neighbouring phenyl group increased from −0.11° to 25.35°. The molecule became more distorted, and a similar twisted intramolecular charge transfer (TICT) effect may have occurred[59-62], which increased the fluorescence nonradiative leap pathway and led to a shorter fluorescence lifetime.

2.6. Erasable Anti-counterfeiting Applications

TPEPhDAT, as an AIE-type fluorescent molecule, skillfully avoids the limitations of ACQ molecules on solid substrates. Therefore, we designed an anti-counterfeiting paper using solution processing. In addition, we have taken advantage of the reversible conversion of fluorescence of **TPEPhDAT** in acidic and alkaline environments and the excellent solubility of acidified **TPEPhDAT** in MeOH for processing and erasure of encrypted information.

To confirm the utility of acid vapour fumigation for fluorescence discolouration under solid substrates. We obtained protonated **TPEPhDAT** samples by direct fumigation with acid vapour in a closed environment (Figure S15a)[63]. The phenomenon was very similar to the change in water, with

 doi:10.20944/preprints202408.0049.v1

nearly 95.7% fluorescence quench and 38 nm redshift (Figure S15b). UV-vis spectra confirmed the redshift in absorption (Figure S15c).

As shown in Figure 6, a QR code written in security ink is stamped on the yellow printing paper. The yellow paper is similar to the colour of the **TPEPhDAT** solid, which can hide the information well and realize that it is unrecognizable under daylight (Figure S16), and only the information can be read under UV light. After fuming with TFA, the fluorescence is quenched under UV light, and the colour changes from green to orange. At the same time, after treatment with NH_3, the fluorescence can be restored entirely, realizing the reversible processing of encrypted information. Finally, it is again treated with an acidic solution. Currently, most of the acidified **TPEPhDAT** can be removed by rinsing with MeOH, thus realizing the erasure of encrypted information under UV light.

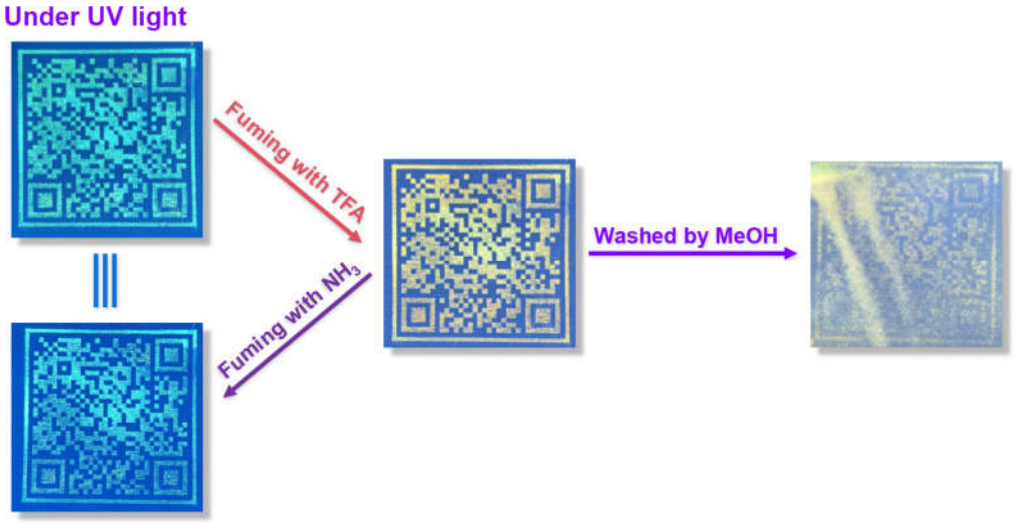

Figure 6. Pictures of reversible fluorescence switching of **TPEPhDAT** in acidic and alkaline environments and its erasure by MeOH (under UV light).

3. Materials and Methods

3.1. Materials

1,1,2,2-tetrakis(4-bromophenyl)ethene, tetrakis(triphenylphosphine)palladium [$Pd(PPh_3)_4$], 4-cyanophenylboronic acid, and 2-methoxyethanol were supplied by Adamas (Shanghai, China). Sodium carbonate (Na_2CO_3), potassium carbonate (K_2CO_3), sodium sulfate (Na_2SO_4), sodium hydroxide (NaOH), dicyandiamide, sulfuric acid (H_2SO_4), dichloromethane (DCM), hydrochloric acid (HCl), methanol (MeOH), ethanol (EtOH), and silica gel were supplied by Greagent (Shanghai, China). Trifluoroacetic acid (TFA), ammonium hydroxide ($NH_3{\cdot}H_2O$), nitric acid (HNO_3), formic acid (FA), and tetrahydrofuran (THF) were supplied by Shanghai Hushi Chemical Co., Ltd. (Shanghai, China). Petroleum ether (PE) was supplied by Shanghai Titan Technology Co., Ltd. (Shanghai, China).

3.1.1. Synthesis of tetrakis[4-(4'-cyanophenyl)phenyl]ethene (**TPEPhCN**)

In a 500 mL round-bottomed flask, 1,1,2,2-tetrakis(4-bromophenyl)ethene (2.5 g, 3.86 mmol), Na_2CO_3 (1 g, 9.43 mmol), 4-cyanophenylboronic acid (3.13 g, 21.28 mmol), and $Pd(PPh_3)_4$ (127 mg, 0.11 mmol) were added to a mixed solvent system consisting of THF (100 mL) and distilled water (50 mL) in the mixture. The mixture was stirred at 100°C for 24 h under a nitrogen atmosphere. The mixture was cooled to room temperature. Quench the mixture with 10% K_2CO_3 solution (30 mL). Extract the mixture with DCM (50 mL × 3). The organic layer was collected, washed twice with saturated saline, and dried with anhydrous Na_2SO_4. The filtrate was filtered and concentrated under reduced pressure. The crude material was purified by silica gel column chromatography using PE and DCM as elution solvents (PE/DCM = 4:1). Removal of the solvent gave a pale yellow solid in 59%

 doi:10.20944/preprints202408.0049.v1

yield. ^{1}H NMR (400 MHz, $CDCl_3$) δ 7.67 (dd, J = 8.7 Hz, 16H), 7.42 (d, J = 8.4 Hz, 8H), 7.21 (d, J = 8.4 Hz, 8H).

3.1.2. Synthesis of 6,6',6'',6'''-(ethene-1,1,2,2-tetrayltetrakis([1,1'-biphenyl]-4',4-diyl))tetrakis(1,3,5-triazine-2,4-diamine) (**TPEPhDAT**)

In a 500 mL round-bottomed flask, tetrakis[4-(4'-cyanophenyl)phenyl]ethene (1 g, 1.36 mmol), NaOH (1 g, 25 mmol), and dicyandiamide (0.5 g, 5.95 mmol) were added to 2-methoxyethanol (40 mL) and stirred at 125°C for 36 h under a nitrogen atmosphere. The mixture was then cooled to room temperature and poured into MeOH. The precipitated solid was filtered, washed with DCM and boiling water, respectively, and dried under vacuum at 90 °C to give a yellowish solid in 80% yield. ^{1}H NMR (400 MHz, DMSO-d_6) δ 8.28 (d, J = 7.7 Hz, 8H), 7.75 (d, J = 7.9 Hz, 8H), 7.63 (d, J = 7.7 Hz, 8H), 7.20 (d, J = 7.6 Hz, 8H), 6.74 (s, 16H).

3.1.3. Synthesis of **TPEPhDAT**-TFA single crystalline

6 mg of **TPEPhDAT** was added to a 2 mL vial containing 200 μL of TFA, followed by 80 μL of EtOH, capped and placed in an oven at 70°C. After 12 h, the orange single crystals were collected for single-crystal X-ray diffraction analysis.

Details of the crystal data, data collection, structure solution, and refinement are shown in Table S1. CCDC 2345516 contains the supplementary crystallographic data for this paper. These data can be obtained free of charge via http://www.ccdc.cam.ac.uk/conts/retrieving.html

3.1.4. The Fabrication of Anti-Counterfeiting Inks

20 mg of **TPEPhDAT** was taken and ground thoroughly for 10 min. Then, 20 mL of EtOH was added and sonicated for 15 min to ensure the solids were well dispersed.

3.1.5. Density Functional Theory (DFT) Calculations

All the DFT calculations were carried out using the Gaussian 16 (version C.01) package. The ground-state geometries were optimized under the B3LYP/6-31G(d,p) level. The DFT-D3 dispersion correction with BJ-damping was applied to correct the weak interaction to improve the calculation accuracy. The IEFPCM implicit solvation model was used to account for the solvation effect. The absorption properties were obtained by time-dependent density functional theory (TDDFT) with the B3LYP function at the same basis set level. Orbital energy level analysis and Electron excitation analysis were performed using Multiwfn software.

3.2. Methods

Solution ^{1}H and ^{13}C NMR spectra were collected by Bruker AVANCE III 400 MHz spectrometers (Bruker Corporation, German). The ^{13}C NMR spectra of **TPEPhDAT** was tested in DMSO-d_6 with the addition of 10 equivalent TFA. X-ray single crystal diffraction was collected by BL17B1 High throughput Protein Crystallography Beamline in Shanghai Synchrotron Radiation Facility and Bruker D8 Venture MetalJet X-ray diffractometer equipped with a Photon II detector (Bruker Corporation, German). Fourier-Transform Infrared (FT-IR) spectra were collected by Thermo Fisher Nicolet iS10 (Thermo Fisher Corporation, America). PL spectra were recorded on a Hitachi F-7000 fluorescence spectrometer (Hitachi Corporation, Japan). Photoluminescence lifetime was obtained on FLS1000 (Edinburg Instruments, Livingstone, UK). Solid ultraviolet-visible (UV-vis) spectra were tested with a Lambda 650S UV-vis spectrophotometer (PERKIN ELMER, America). Liquid UV-vis spectra were tested by a UV-9000S UV-vis spectrophotometer (METASH, China). Dynamic light scattering (DLS) was examined on a Nano-ZS90 (Malvern Instruments, England). Scanning electron microscope (SEM) images were obtained on a LaB_6 VEGA 3 XMU scanning electron microscope (TESCAN, Czech Republic) at an acceleration voltage of 200 V − 30 kV.

 doi:10.20944/preprints202408.0049.v1

4. Conclusions

This paper reports a DAT group-modified TPE molecule, **TPEPhDAT**, prepared by Suzuki-Miyaura coupling and cyclization reactions. The DMSO/MeOH system exhibits excellent AIE properties, and the luminescence intensity of its solid-state aggregates is about five times higher than that of dilute solutions. Since the triazine ring is easily protonated, **TPEPhDAT** exhibits an apparent acid-induced fluorescence discolouration behaviour. The protonation occurred on the triazine ring rather than $-NH_2$, as confirmed by various means, including ^1H NMR, FT-IR, single crystals, etc. Reversible switching between yellow and orange-red fluorescence is achieved by using alternating treatment of TFA with ammonia. TDDFT calculations show that the electron-withdrawing capacity of the triazine unit is enhanced after TFA protonation, leading to a decrease in the band gap and a change in the distribution of the electron cloud, which is the fundamental cause of the wavelength redshift and fluorescence quenching. Based on their acid-induced discolouration behaviour and the property that MeOH can quickly shift them out after protonation, they are processed into paper with encrypted information for anti-counterfeiting by solution method. It can be seen that this property of reversible switching of fluorescence under alternating acid-base stimulation makes the molecule potentially applicable in the field of information processing and anti-counterfeiting.

Supplementary Materials: The following supporting information can be downloaded at: www.mdpi.com/xxx/s1, Figure S1: ^1H NMR spectra of **TPEPhCN**; Figure S2: ^1H NMR spectra of **TPEPhDAT**; Figure S3: ^{13}C NMR spectra of **TPEPhDAT**; Figure S4: Localized enlarged ^{13}C NMR spectra of **TPEPhDAT**; Figure S5: UV-vis absorption spectra of **TPEPhDAT** in solution (f_{MeOH} = 0 vol%) and aggregate (f_{MeOH} = 95 vol%); Figure S6: SEM pictures of aggregates at f_{MeOH} = 95 vol%; Figure S7: Emission spectra of **TPEPhDAT** dispersed in water (2 mL) before and after the addition of aqueous solution of (**a**) H_2SO_4 (200 μL, 0.25 M), (**b**) HCl (200 μL, 0.5 M), (**c**) FA (200 μL, 0.5 M), (**d**) TFA (200 μL, 0.5 M) and (**e**) HNO_3 (200 μL, 0.5 M); Figure S8: Absolute quantum yield of **TPEPhDAT** before and after addition of various acids; Figure S9: The possible structure of the protonated triazine ring; Figure S10: Electrostatic potentials mapped on isodensity surfaces of **TPEPhDAT**; Figure S11: Microscopic optical image for **TPEPhDAT-TFA**; Figure S12: Schematic representation of **TPEPhDAT** after protonation by TFA; Figure S13: Calculated absorption energy of bared and protonated **TPEPhDAT** monomer; Figure S14: Dihedral angle between triazine ring and neighboring benzene ring before and after **TPEPhDAT** protonation; Figure S15: (**a**) Schematic diagram of **TPEPhDAT** fumigated TFA. Fluorescence spectra (**b**) and UV-vis absorption spectra (**c**) of **TPEPhDAT** before and after fumigation of TFA; Figure S16: Pictures of reversible switching of fluorescence of **TPEPhDAT** in acidic and alkaline environments and its erasure by MeOH (under daylight); Table S1: Crystallographic data of **TPEPhDAT-TFA**.

Author Contributions: Conceptualization, Z.L. and P.L.; methodology, J.L. and X.G.; software, J.L. and Q.N.; validation, J.L., X.G. and Q.N.; formal analysis, J.L., X.G., Q.N., M.J. and Y.W.; investigation, J.L. and X.G.; resources, Z.L., P.L., H.S. and B.C.; data curation, J.L., M.J. and Y.W.; writing—original draft preparation, J.L.; writing—review and editing, J.L., Z.L. and P.L.; visualization, Z.L. and P.L.; supervision, P.L. and Z.L.; project administration, P.L. and Z.L.; funding acquisition, T.A. All authors have read and agreed to the published version of the manuscript.

Funding: This research was funded by the Princess Nourah bint Abdulrahman University Researchers Supporting Project number (HCPNU2024R1), Princess Nourah bint Abdulrahman University, Riyadh, Saudi Arabia.

Institutional Review Board Statement: Not applicable.

Informed Consent Statement: Not applicable.

Data Availability Statement: The data presented in this study are available on request from the corresponding author.

Acknowledgments: We thank the staff at SSRF BL17B1 of the National Facility for Protein Science in Shanghai (NFPS), Shanghai Advanced Research Institute, CAS, for technical support in X-ray diffraction data collection and analysis.

Conflicts of Interest: The authors declare no conflicts of interest.

 doi:10.20944/preprints202408.0049.v1

References

1. Tong, S.; Dai, J.; Sun, J.; Liu, Y.; Ma, X.; Liu, Z.; Ma, T.; Tan, J.; Yao, Z.; Wang, S.; et al. Fluorescence-based monitoring of the pressure-induced aggregation microenvironment evolution for an AIEgen under multiple excitation channels. *Nat. Commun.* **2022**, *13*, 5234, doi:10.1038/s41467-022-32968-9.
2. Chen, C.X.; Yin, S.Y.; Wei, Z.W.; Qiu, Q.F.; Zhu, N.X.; Fan, Y.N.; Pan, M.; Su, C.Y. Pressure-Induced Multiphoton Excited Fluorochromic Metal-Organic Frameworks for Improving MPEF Properties. *Angew. Chem. Int. Ed.* **2019**, *58*, 14379–14385, doi:10.1002/anie.201908793.
3. Nagasawa, H.; Kagawa, T.; Noborio, T.; Kanezashi, M.; Ogata, A.; Tsuru, T. Ultrafast Synthesis of Silica-Based Molecular Sieve Membranes in Dielectric Barrier Discharge at Low Temperature and Atmospheric Pressure. *J. Am. Chem. Soc.* **2020**, *143*, 35–40, doi:10.1021/jacs.0c09433.
4. Hu, D.; Xu, W.; Wang, G.; Liu, K.; Wang, Z.; Shi, Q.; Lin, S.; Liu, Z.; Fang, Y. A Mild-Stimuli-Responsive Fluorescent Molecular System Enables Multilevel Anti-Counterfeiting and Highly Adaptable Temperature Monitoring. *Adv. Funct. Mater.* **2022**, *32*, 2207895, doi:10.1002/adfm.202207895.
5. Shen, F.; Yang, W.; Cui, J.; Hou, Y.; Bai, G. Small-Molecule Fluorogenic Probe for the Detection of Mitochondrial Temperature In Vivo. *Anal. Chem.* **2021**, *93*, 13417–13420, doi:10.1021/acs.analchem.1c03554.
6. Zhang, Q.; Yang, L.; Han, Y.; Wang, Z.; Li, H.; Sun, S.; Xu, Y. A pH-sensitive ESIPT molecule with aggregation-induced emission and tunable solid-state fluorescence multicolor for anti-counterfeiting and food freshness detection. *Chem. Eng. J.* **2022**, *428*, 130986, doi:10.1016/j.cej.2021.130986.
7. Hisaki, I.; Suzuki, Y.; Gomez, E.; Ji, Q.; Tohnai, N.; Nakamura, T.; Douhal, A. Acid Responsive Hydrogen-Bonded Organic Frameworks. *J. Am. Chem. Soc.* **2019**, *141*, 2111–2121, doi:10.1021/jacs.8b12124.
8. Li, Z.; Liu, X.; Wang, G.; Li, B.; Chen, H.; Li, H.; Zhao, Y. Photoresponsive supramolecular coordination polyelectrolyte as smart anticounterfeiting inks. *Nat. Commun.* **2021**, *12*, 1363, doi:10.1038/s41467-021-21677-4.
9. Wang, G.; Feng, Y.; Ye, X.; Li, Z.; Tao, S.; Jiang, D. Light-Gating Crystalline Porous Covalent Organic Frameworks. *J. Am. Chem. Soc.* **2024**, *146*, 10953–10962, doi:10.1021/jacs.4c02164.
10. Zhang, J.-H.; Wang, H.-P.; Zhang, L.-Y.; Wei, S.-C.; Wei, Z.-W.; Pan, M.; Su, C.-Y. Coordinative-to-covalent transformation, isomerization dynamics, and logic gate application of dithienylethene based photochromic cages. *Chem. Sci.* **2020**, *11*, 8885–8894, doi:10.1039/d0sc03290e.
11. Ding, Y.; Guo, J.; He, X.; Tao, W.; Shi, Y.; Xu, J.; Xu, L.; Tang, M.; Shen, D.; Bi, H.; et al. Tuned Intra- and Intermolecular Photoreactions of Tridentate Cyanostilbenes with Distinct Aggregated-State Photomechanical and Dispersed-State Photochromic Behaviors. *Adv. Funct. Mater.* **2023**, *33*, 2212886, doi:10.1002/adfm.202212886.
12. Hu, Z.B.; Li, L.H.; Han, Y.; Zhang, J.; Li, J.; Chen, Z.; Wu, S.; Zhang, Y.; Ye, H.Y.; Song, Y. A new insight into the unique magneto-optical effect of layered perovskite $(C_6H_5C_2H_3FNH_3)_2MnCl_4$. *Aggregate* **2022**, *4*, e294, doi:10.1002/agt2.294.
13. Wei, W.; He, L.; Han, G.; Lu, Y.; Shi, S.; Yuan, Z.; Wang, X.; Li, Y.; Chen, B.; Zhang, Z.; et al. Stimulus-responsive hydrogen-bonded organic frameworks: Construction strategies, research progress and applications. *Coord. Chem. Rev.* **2024**, *507*, 215760, doi:10.1016/j.ccr.2024.215760.
14. Shi, Y.; Wang, S.; Tao, W.; Guo, J.; Xie, S.; Ding, Y.; Xu, G.; Chen, C.; Sun, X.; Zhang, Z.; et al. Multiple yet switchable hydrogen-bonded organic frameworks with white-light emission. *Nat. Commun.* **2022**, *13*, 1882, doi:10.1038/s41467-022-29565-1.
15. Wei, P.; He, X.; Zheng, Z.; He, D.; Li, Q.; Gong, J.; Zhang, J.; Sung, H.H.Y.; Williams, I.D.; Lam, J.W.Y.; et al. Robust Supramolecular Nano-Tunnels Built from Molecular Bricks**. *Angew. Chem. Int. Ed.* **2021**, *60*, 7148–7154, doi:10.1002/anie.202013117.
16. Zhang, T.L.; Zhao, C.; Liu, Z.J.; Xu, T.Y.; Lin, H.Y.; Zhou, S.W.; Li, Y.H.; Tong, F. Reversible Acid-Base Responsive Fluorescence Changes of Solutions and Crystals Based on Anthracenyl Pyridyl Derivatives. *ChemPhotoChem* **2023**, *7*, e202300194, doi:10.1002/cptc.202300194.
17. Zeng, C.Y.; Deng, W.J.; Zhao, K.Q.; Redshaw, C.; Donnio, B. Phenanthrothiophene-Triazine Star-Shaped Discotic Liquid Crystals: Synthesis, Self-Assembly, and Stimuli-Responsive Fluorescence Properties. *Chem. - Eur. J.* **2024**, *30*, e202400296, doi:10.1002/chem.202400296.
18. Yang, J.; Chen, M.; Li, P.; Cheng, F.; Xu, Y.; Li, Z.; Wang, Y.; Li, H. Self-healing hydrogel containing Eu-polyoxometalate as acid-base vapor modulated luminescent switch. *Sens. Actuators, B* **2018**, *273*, 153–158, doi:10.1016/j.snb.2018.06.024.
19. Yang, J.; Wang, T.; Guo, R.; Yao, D.; Guo, W.; Liu, S.; Li, Z.; Wang, Y.; Li, H. Self-Healing Material with Reversible Luminescence Switch Behavior. *ACS Appl. Mater. Interfaces* **2020**, *12*, 54026–54034, doi:10.1021/acsami.0c13509.
20. Kalita, A.; Malik, A.H.; Sarma, N.S. Stimuli-Responsive Naphthalene Diimide as Invisible Ink: A Rewritable Fluorescent Platform for Anti-Counterfeiting. *Chem. - Asian J.* **2020**, *15*, 1074–1080, doi:10.1002/asia.201901800.

21. Wu, J.; Jiao, X.; Chen, D.; Li, C. Dual-stimuli responsive color-changing nanofibrous membranes as effective media for anti-counterfeiting and erasable writing. *Colloids Surf., A* **2021**, *621*, 126626, doi:10.1016/j.colsurfa.2021.126626.
22. Li, M.; Li, X.; Huang, L.; Song, R.; Yang, J.; Zhang, H. A novel photochromic complex based on a viologen ligand with rapid inkless and erasable printing, anti-counterfeiting and amine-selective responses. *Inorg. Chem. Commun.* **2023**, *153*, 110839, doi:10.1016/j.inoche.2023.110839.
23. Yu, C.-M.; Wang, P.-H.; Liu, Q.; Cai, L.-Z.; Guo, G.-C. Modulating Fading Time of Photochromic Compounds by Molecular Design for Erasable Inkless Printing and Anti-counterfeiting. *Cryst. Growth Des.* **2021**, *21*, 1323–1328, doi:10.1021/acs.cgd.0c01597.
24. Hong, Y.; Lam, J.W.Y.; Tang, B.Z. Aggregation-induced emission. *Chem. Soc. Rev.* **2011**, *40*, 5361–5388, doi:10.1039/c1cs15113d.
25. Hu, R.; Leung, N.L.C.; Tang, B.Z. AIE macromolecules: syntheses, structures and functionalities. *Chem. Soc. Rev.* **2014**, *43*, 4494–4562, doi:10.1039/c4cs00044g.
26. Li, P.; He, Y.; Arman, H.D.; Krishna, R.; Wang, H.; Weng, L.; Chen, B. A microporous six-fold interpenetrated hydrogen-bonded organic framework for highly selective separation of C_2H_4/C_2H_6. *Chem. Commun.* **2014**, *50*, 13081–13084, doi:10.1039/c4cc05506c.
27. Wang, H.; Li, B.; Wu, H.; Hu, T.-L.; Yao, Z.; Zhou, W.; Xiang, S.; Chen, B. A Flexible Microporous Hydrogen-Bonded Organic Framework for Gas Sorption and Separation. *J. Am. Chem. Soc.* **2015**, *137*, 9963–9970, doi:10.1021/jacs.5b05644.
28. Song, C.-L.; Li, Z.; Wu, J.-R.; Lu, T.; Yang, Y.-W. Intramolecular Through-Space Interactions Induced Emission of Pillar[4]arene[1]dicyanobenzene. *Chem. Mater.* **2022**, *34*, 10181–10189, doi:10.1021/acs.chemmater.2c03025.
29. Yu, Y.; Xing, H.; Zhou, Z.; Liu, J.; Sung, H.H.Y.; Williams, I.D.; Halpert, J.E.; Zhao, Z.; Tang, B.Z. How do molecular interactions affect fluorescence behavior of AIEgens in solution and aggregate states? *Sci. China Chem.* **2021**, *65*, 135–144, doi:10.1007/s11426-021-1083-4.
30. Lee, M.M.S.; Yu, E.Y.; Yan, D.; Chau, J.H.C.; Wu, Q.; Lam, J.W.Y.; Ding, D.; Kwok, R.T.K.; Wang, D.; Tang, B.Z. The Role of Structural Hydrophobicity on Cationic Amphiphilic Aggregation-Induced Emission Photosensitizer-Bacterial Interaction and Photodynamic Efficiency. *ACS Nano* **2023**, *17*, 17004–17020, doi:10.1021/acsnano.3c04266.
31. Tu, Y.; Yu, Y.; Xiao, D.; Liu, J.; Zhao, Z.; Liu, Z.; Lam, J.W.Y.; Tang, B.Z. An Intelligent AIEgen with Nonmonotonic Multiresponses to Multistimuli. *Adv. Sci.* **2020**, *7*, 2001845, doi:10.1002/advs.202001845.
32. Zhang, J.; Tu, Y.; Shen, H.; Lam, J.W.Y.; Sun, J.; Zhang, H.; Tang, B.Z. Regulating the proximity effect of heterocycle-containing AIEgens. *Nat. Commun.* **2023**, *14*, 3772, doi:10.1038/s41467-023-39479-1.
33. Zhang, Y.; Sun, J.; Bian, G.; Chen, Y.; Ouyang, M.; Hu, B.; Zhang, C. Cyanostilben-based derivatives: mechanical stimuli-responsive luminophors with aggregation-induced emission enhancement. *Photochem. Photobiol. Sci.* **2012**, *11*, 1414–1421, doi:10.1039/c2pp05404c.
34. Shi, J.; Zhang, S.; Zheng, M.; Deng, Q.; Zheng, C.; Li, J.; Huang, F. A novel fluorometric turn-on assay for lipase activity based on an aggregation-induced emission (AIE) luminogen. *Sens. Actuators, B* **2017**, *238*, 765–771, doi:10.1016/j.snb.2016.07.116.
35. Zhang, H.; Zhao, Z.; Turley, A.T.; Wang, L.; McGonigal, P.R.; Tu, Y.; Li, Y.; Wang, Z.; Kwok, R.T.K.; Lam, J.W.Y.; et al. Aggregate Science: From Structures to Properties. *Adv. Mater.* **2020**, *32*, 2001457, doi:10.1002/adma.202001457.
36. Mei, J.; Hong, Y.; Lam, J.W.Y.; Qin, A.; Tang, Y.; Tang, B.Z. Aggregation-Induced Emission: The Whole Is More Brilliant than the Parts. *Adv. Mater.* **2014**, *26*, 5429–5479, doi:10.1002/adma.201401356.
37. Jing, H.; Lu, L.; Feng, Y.; Zheng, J.-F.; Deng, L.; Chen, E.-Q.; Ren, X.-K. Synthesis, Aggregation-Induced Emission, and Liquid Crystalline Structure of Tetraphenylethylene–Surfactant Complex via Ionic Self-Assembly. *J. Phys. Chem. C* **2016**, *120*, 27577–27586, doi:10.1021/acs.jpcc.6b09901.
38. Tang, B.Z.; Geng, Y.; Lam, J.W.Y.; Li, B.; Jing, X.; Wang, X.; Wang, F.; Pakhomov, A.B.; Zhang, X.X. Processible Nanostructured Materials with Electrical Conductivity and Magnetic Susceptibility: Preparation and Properties of Maghemite/Polyaniline Nanocomposite Films. *Chem. Mater.* **1999**, *11*, 1581–1589, doi:10.1021/cm9900305.
39. Gao, M.; Hong, Y.; Chen, B.; Wang, Y.; Zhou, W.; Wong, W.W.H.; Zhou, J.; Smith, T.A.; Zhao, Z. AIE conjugated polyelectrolytes based on tetraphenylethene for efficient fluorescence imaging and lifetime imaging of living cells. *Polym. Chem.* **2017**, *8*, 3862–3866, doi:10.1039/c7py00564d.
40. Kuimova, M.K.; Yahioglu, G.; Levitt, J.A.; Suhling, K. Molecular Rotor Measures Viscosity of Live Cells via Fluorescence Lifetime Imaging. *J. Am. Chem. Soc.* **2008**, *130*, 6672–6673, doi:10.1021/ja800570d.
41. Han, Y.; Zhang, T.; Chen, X.; Chen, Q.; Hao, J.; Song, W.; Zeng, Y.; Xue, P. Guest-Regulated Luminescence and Force-Stimuli Response of a Hydrogen-Bonded Organic Framework. *ACS Appl. Mater. Interfaces* **2021**, *13*, 32270–32277, doi:10.1021/acsami.1c08316.

42. Zadehnazari, A.; Khosropour, A.; Altaf, A.A.; Rosen, A.S.; Abbaspourrad, A. Tetrazine-Linked Covalent Organic Frameworks With Acid Sensing and Photocatalytic Activity. *Adv. Mater.* **2024**, *36*, 2311042, doi:10.1002/adma.202311042.
43. Becker, E.D.; Miles, H.T.; Bradley, R.B. Nuclear Magnetic Resonance Studies of Methyl Derivatives of Cytosine. *J. Am. Chem. Soc.* **2002**, *87*, 5575–5582, doi:10.1021/ja00952a011.
44. Miles, H.T.; Bradley, R.B.; Becker, E.D. Tautomerism and Site of Protonation of 1-Methylcytosine: Proof by Nuclear Magnetic Resonance Spin-Spin Coupling. *Science* **1963**, *142*, 1569–1571, doi:10.1126/science.142.3599.1569.
45. Xu, J.; Wu, G.; Wang, Z.; Zhang, X. Generation of 2D organic microsheets from protonated melamine derivatives: suppression of the self assembly of a particular dimension by introduction of alkyl chains. *Chem. Sci.* **2012**, *3*, 3227–3230, doi:10.1039/c2sc20871g.
46. Perpétuo, G.J.; Janczak, J. Solid-state supramolecular architectures formed by co-crystallization of melamine and 2-, 3- and 4-fluorophenylacetic acids. *J. Mol. Struct.* **2018**, *1152*, 237–247, doi:10.1016/j.molstruc.2017.09.099.
47. Marchewka, M.K.; Pietraszko, A.; Feki, H.; Abid, Y. Crystal structure and vibrational spectra of melaminium 2,5-dinitrophenolate monohydrate: FT-IR, FT-Raman and quantum chemical calculations. *Vib. Spectrosc.* **2011**, *56*, 255–264, doi:10.1016/j.vibspec.2011.03.006.
48. Song, X.; Wang, Y.; Wang, C.; Gao, X.; Zhou, Y.; Chen, B.; Li, P. Self-Healing Hydrogen-Bonded Organic Frameworks for Low-Concentration Ammonia Capture. *J. Am. Chem. Soc.* **2023**, *146*, 627–634, doi:10.1021/jacs.3c10492.
49. Gündüz, T.; Gündüz, N.; Kılıç, E.; Kenar, A. Titrations in non-aqueous media. Part III. Basicity order of aniline, *N*-Alkyl- and *N*-aryl-substituted anilines and pyridine in nitrobenzene solvent. *The Analyst* **1986**, *111*, 1103–1105, doi:10.1039/an9861101103.
50. Dzidic, I. Relative gas-phase basicities of some amines, anilines, and pyridines. Application of some Broensted acids as reactants in chemical ionization mass spectrometry. *J. Am. Chem. Soc.* **2002**, *94*, 8333–8335, doi:10.1021/ja00779a009.
51. Mucci, A.; Domain, R.; Benoit, R.L. Solvent effect on the protonation of some alkylamines. *Can. J. Chem.* **1980**, *58*, 953–958, doi:10.1139/v80-151.
52. Benoit, R.L.; Mackinnon, M.J.; Bergeron, L. Basicity of N-substituted anilines and pyridine in dimethylsulfoxide. *Can. J. Chem.* **1981**, *59*, 1501–1504, doi:10.1139/v81-220.
53. Lv, Y.; Liang, J.; Xiong, Z.; Yang, X.; Li, Y.; Zhang, H.; Xiang, S.; Chen, B.; Zhang, Z. Smart-Responsive HOF Heterostructures with Multiple Spatial-Resolved Emission Modes toward Photonic Security Platform. *Adv. Mater.* **2023**, *36*, 2309130, doi:10.1002/adma.202309130.
54. Zheng, P.; Abdurahman, A.; Liu, G.; Liu, H.; Zhang, Y.; Zhang, M. An instantaneously-responded, ultrasensitive, reutilizable fluorescent probe to sarin substitute both in solution and in gas phase. *Sens. Actuators, B* **2020**, *322*, 128611, doi:10.1016/j.snb.2020.128611.
55. Zheng, P.; Abdurahman, A.; Zhang, Z.; Feng, Y.; Zhang, Y.; Ai, X.; Li, F.; Zhang, M. A simple organic multi-analyte fluorescent prober: One molecule realizes the detection to DNT, TATP and Sarin substitute gas. *J. Hazard. Mater.* **2021**, *409*, 124500, doi:10.1016/j.jhazmat.2020.124500.
56. Liu, Y.; Yan, B. Configuration-regulated highly luminescent hydrogen-organic frameworks for detection of phenelzine and propofol. *Inorg. Chem. Front.* **2024**, *11*, 1099–1107, doi:10.1039/d3qi02083e.
57. Gu, K.; Meng, Z.; Liu, X.; Wu, Y.; Qi, X.; Ren, Y.; Yu, Z.-Q.; Tang, B.Z. A gated strategy stabilizes room-temperature phosphorescence. *Aggregate* **2023**, *4*, e337, doi:10.1002/agt2.337.
58. Shen, H.; Li, Y.; Li, Y. Self-assembly and tunable optical properties of intramolecular charge transfer molecules. *Aggregate* **2020**, *1*, 57–68, doi:10.1002/agt2.6.
59. Hanaoka, K.; Iwaki, S.; Yagi, K.; Myochin, T.; Ikeno, T.; Ohno, H.; Sasaki, E.; Komatsu, T.; Ueno, T.; Uchigashima, M.; et al. General Design Strategy to Precisely Control the Emission of Fluorophores via a Twisted Intramolecular Charge Transfer (TICT) Process. *J. Am. Chem. Soc.* **2022**, *144*, 19778–19790, doi:10.1021/jacs.2c06397.
60. Lee, J.m.; Yuk, S.b.; Namgoong, J.w.; Kim, J.p. Mechanofluorochromism of Triphenylamine-BODIPY: Effect of twisted intramolecular charge transfer and restriction in rotation on fluorescence. *Dyes Pigm.* **2021**, *185*, 108864, doi:10.1016/j.dyepig.2020.108864.
61. Sasaki, S.; Drummen, G.P.C.; Konishi, G.-i. Recent advances in twisted intramolecular charge transfer (TICT) fluorescence and related phenomena in materials chemistry. *J. Mater. Chem. C* **2016**, *4*, 2731–2743, doi:10.1039/c5tc03933a.
62. Zhang, W.; Kong, J.; Miao, R.; Song, H.; Ma, Y.; Zhou, M.; Fang, Y. Integrating Aggregation Induced Emission and Twisted Intramolecular Charge Transfer via Molecular Engineering. *Adv. Funct. Mater.* **2023**, *34*, 2311404, doi:10.1002/adfm.202311404.
63. Xia, G.; Jiang, Z.; Shen, S.; Liang, K.; Shao, Q.; Cong, Z.; Wang, H. Reversible Specific Vapoluminescence Behavior in Pure Organic Crystals through Hydrogen-Bonding Docking Strategy. *Adv. Opt. Mater.* **2019**, *7*, 1801549, doi:10.1002/adom.201801549.

 doi:10.20944/preprints202408.0049.v1